Neural Network-Based Secure Beam Management in 5G Networks for Cyberspace Protection

Juliy Boiko[1,*,†] and Ilya Pyatin[2,†]

[1] *Khmelnytskyi National University, 11, Instytuts'ka str., Khmelnytskyi, 29016, Ukraine*

[2] *Khmelnytskyi Polytechnic Professional College by Lviv Polytechnic National University, 10, Zarichanska str., Khmelnytskyi, 29019, Ukraine*

Abstract

This paper proposes a neural network-based secure beam management method in fifth-generation (5G) wireless networks to reduce signaling overhead, enhance spatial transmission accuracy, and strengthen communication resilience in cyberspace. A synchronization signal block (SSB) is generated using New Radio (NR) synchronization signals, where each beam scans specific azimuth and elevation directions. The beams propagate through a spatial scattering channel and are received using multiple receive beams. For each transmit-receive beam pair, the reference signal received power (RSRP) is measured to identify the optimal pair with the highest signal strength. Key performance indicators such as RSRP, received signal strength indicator (RSSI), and reference signal signal-to-noise ratio (RSRQ) are analyzed across various bandwidths. A heatmap of RSRP values provides a visual overview of optimal beam pairings. To support secure and intelligent beam selection, a neural network (NN) is trained to predict the best beam pair based on the receiver's position. The network proposes a list of K candidate beam pairs and performs an exhaustive search among them to select the one with the highest average RSRP. By minimizing overhead signaling, the method reduces the attack surface of the control plane. The model is compared with k-nearest neighbors (KNN), statistical, and random selection methods. The NN-based approach, along with statistical and random methods, achieves near 100% accuracy, while KNN lags by approximately 20%. The results confirm the value of NN-driven beam selection in enhancing robust and protected 5G communications.

Keywords

beam management, neural network, secure communication, beam pair selection, 5G, location

1. Introduction

The exponential growth in data demand and the proliferation of connected devices have positioned fifth-generation (5G) wireless networks as the backbone of next-generation mobile communications [1, 2]. As critical infrastructure increasingly relies on wireless connectivity, ensuring secure, resilient, and efficient communication in 5G environments becomes paramount. One of the key technologies enabling high data rates and ultra-low latency in 5G is the use of millimeter-wave (mmWave) frequency bands [3]. However, while mmWave offers wider bandwidth and high throughput, it also introduces new cyber-physical challenges, including vulnerability to jamming, eavesdropping, and link disruption due to severe path loss and signal blockage. These issues affect not only performance but also the integrity and availability of wireless communication channels.

To overcome these physical limitations, beamforming and beam management are essential. These techniques allow directional transmission and reception using multiple antenna arrays, focusing the radio energy towards specific directions. In the context of 5G NR [4], the initial access procedure typically relies on exhaustive beam sweeping, where each possible transmit-receive beam pair is evaluated to identify the one offering the highest RSRP [5, 6]. While this method ensures reliable

Information Technology and Implementation (IT&I-2025), November 20-21, 2025, Kyiv, Ukraine

*Corresponding author.

† These authors contributed equally.

boiko_julius@ukr.net (J. Boiko); ilkhmel@ukr.net (I. Pyatin)

0000-0003-0603-7827 (J. Boiko); 0000-0003-1898-6755 (I. Pyatin)

initial access, it becomes increasingly inefficient and resource-intensive as the number of antennas and beam combinations grows. For example, a system with 64 transmit and 64 receive beams leads to 4096 possible combinations, requiring up to 320 ms for full bidirectional sweeping, which is impractical in dynamic or latency-critical environments.

To address these bottlenecks, recent research has shifted toward smart beam management solutions using machine learning (ML), and particularly NNs [7-9]. These approaches aim to reduce scanning overhead by predicting the most suitable beam pairs based solely on readily available input, such as the user equipment's (UE) GPS coordinates, thereby eliminating the need for exhaustive scanning.

This paper investigates the implementation of a NN-based beam selection framework that predicts the top K candidate beam pairs, significantly reducing access latency and signaling overhead. The model is trained on synthetic data generated through detailed simulation of receiver positions and scattering environments. Each data sample maps a set of UE coordinates to the optimal beam pair index determined through exhaustive search. During inference, the network suggests K promising beam combinations, among which the final choice is made based on RSRP evaluation. Simulation results show that the proposed approach achieves over 90% Top-K accuracy with K=8, cutting scanning delay by up to 75% compared to exhaustive search. Moreover, the predicted beam pairs yield RSRP values nearly equivalent to the true optimum, validating the practicality of the method.

While mmWave technology enables high-throughput communication, its practical deployment is hindered by significant computational complexity, scanning latency, and signaling overhead during beam alignment. Traditional heuristic methods like KNN [10] or frequency-based statistical estimations often lack adaptability and generalization in complex or dynamic propagation environments.

The main objective of this work is to design, train, and evaluate a smart NN model for efficient beam selection in 5G mmWave networks. The focus is on minimizing the beam scanning burden while maintaining high beam selection accuracy and robust signal quality.

To achieve the research objectives, a series of tasks were carried out. First, a synthetic dataset was generated by simulating beam sweeping results for various UE locations. For each receiver position, the optimal beam pair was identified using exhaustive evaluation to serve as ground truth. A NN was then trained to map GPS coordinates of the UE to the corresponding beam pair indices. The model's performance was assessed using metrics such as Top-K classification accuracy and average RSRP. Finally, the proposed method was compared with baseline approaches, including KNN, statistical, and random beam selection methods, to highlight its advantages in terms of accuracy and efficiency.

With the rollout of densely deployed 5G networks [11, 12] and the growing demand for ultra-reliable and low-latency communication (URLLC) [13], the need for intelligent and scalable beam management becomes increasingly critical. The integration of NN's into the beam selection pipeline transforms the traditionally static and computationally intensive procedure into a smart and adaptive process. This approach not only accelerates initial access and improves energy efficiency but also lays the foundation for future wireless systems, including 6G, where real-time learning, context awareness, and AI-driven decision-making will be fundamental to network operation.

2. Beam Management Procedures in 5G NR Systems

Beam management is a critical functionality in 5G NR, particularly in the millimeter wave (mmWave) frequency bands where highly directional transmission and reception are required to overcome severe path losses. The process includes several key procedures such as beam sweeping, beam measurement, beam determination, beam refinement, and beam recovery. These procedures are performed during the initial access and throughout the connection to maintain optimal communication quality.

During the initial access stage (Procedure P-1), the gNB (next-generation Node B) transmits SSBs [14] in the form of a beam-sweeping package across the coverage sector. Concurrently, the UE (User Equipment) scans its reception beams to perform a bidirectional search. For each transmitter–receiver beam pair, the RSRP is measured at the physical layer. Based on the RSRP measurements, the system determines the optimal transmit–receive beam pair. At the MAC layer, the UE reports the strongest beam pairs (Beam Reporting) to the gNB. Once a suitable beam pair is established, it is locked for future data transmission and control signaling. In the case of a link failure, the system may initiate re-scanning or switch to a backup beam, enabling robust Beam Recovery.

Figure 1 illustrates the core steps of the initial access procedure (P-1), along with beam refinement methods P-2 and P-3.

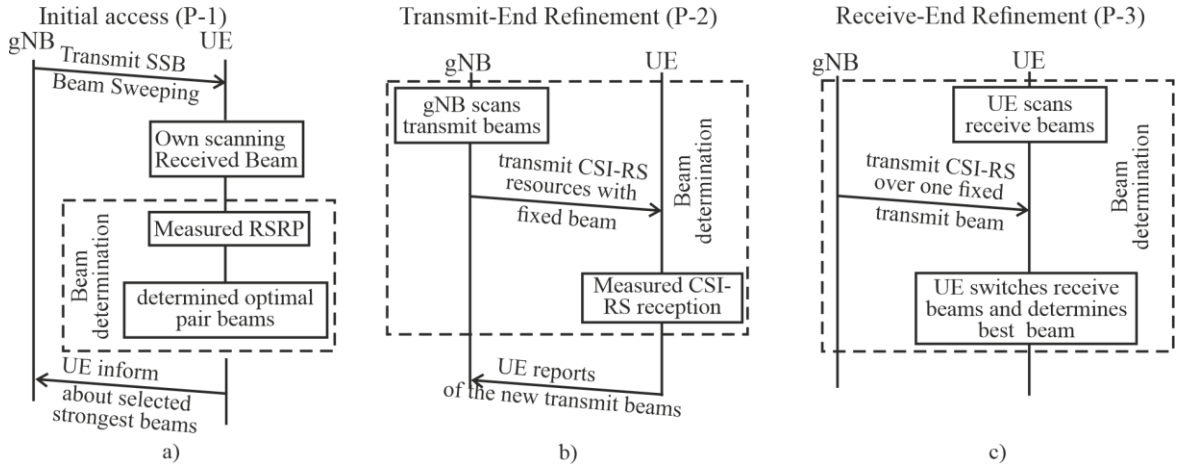

Figure 1: Core steps of the initial access procedure (P-1), along with transmit- and receive-side beam refinement methods (P-2 and P-3).

After initial access, beam refinement is essential for optimizing the transmission link, especially in dynamic or high-mobility scenarios. Procedure P-2 (Transmit-End Refinement) involves the gNB performing a fine-grained scan of transmit beams using Channel State Information Reference Signals (CSI-RS). These signals are transmitted with the UE's receive beam fixed. The UE measures RSRP values and reports the best performing transmit beam. Procedure P-3 (Receive-End Refinement), conversely, fixes the gNB's transmit beam and allows the UE (or gNB, in uplink) to scan its receive beams. CSI-RS (for DL) or Sounding Reference Signals (SRS) (for UL) are used for beam quality assessment, enabling selection of the optimal receive beam.

In cases of link degradation or beam failure, Beam Failure Recovery (BFR) is activated. This involves either reusing previously measured backup beams or re-initiating P-1 sweeping to find a new suitable beam pair. BFR ensures communication continuity even under mobility or blockage conditions.

Traditional P-1 procedures involve exhaustive sweeping of all possible beam pairs, which becomes computationally intensive as the number of antennas increases. ML techniques can dramatically reduce this overhead. By using input data such as UE GPS coordinates, a NN can predict the top K most promising beam pairs, thereby reducing the number of measurements required.

ML-based prediction modules can replace the traditional exhaustive sweeping block during:

- initial Access (P-1). (ML reduces beam search space and accelerates access time).
- beam Recovery. (In case of beam failure, the model quickly suggests new candidate beam pairs based on context).

Figure 2 presents the detailed signal processing stages for P-1. Beam management functions are highlighted for clarity.

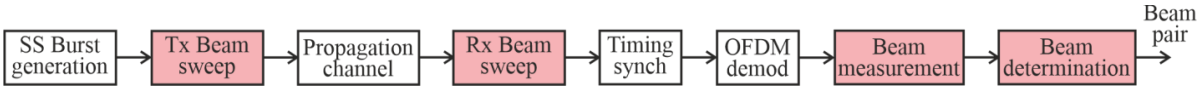

Figure 2: Detailed signal processing stages of the initial access procedure (P-1).

We investigated the NR SSB beam sweeping simulation model. The simulation setup incorporates a variety of configurable parameters that define the beam sweeping environment and signal acquisition behavior. These include the cell identity (Cell ID), the selected frequency range—either FR1 or FR2—and the corresponding central carrier frequency. The SSB pattern is chosen based on the frequency range: types A, B, or C for FR1, and types D or E for FR2, with each pattern implicitly determining the subcarrier spacing. The number of transmitted SSBs also varies, with typical configurations of 4 or 8 beams for FR1 and up to 64 beams for FR2. Transmit and receive antenna arrays are modeled as Uniform Rectangular Arrays (URA), with independently configurable horizontal and vertical dimensions. Beam scanning is conducted across specified azimuth and elevation ranges, with optional activation of elevation sweeping. Additionally, the simulation accounts for signal-to-noise ratio (SNR) in decibels and supports different reference RSRP measurement modes—such as 'SSSonly' or 'SSSwDMRS'—to evaluate synchronization signal quality.

Figure 3 shows a spectrogram of the synchronization signal package at 35 GHz. Figures 4 a and 4 b illustrate the transmit and receive array response patterns, respectively.

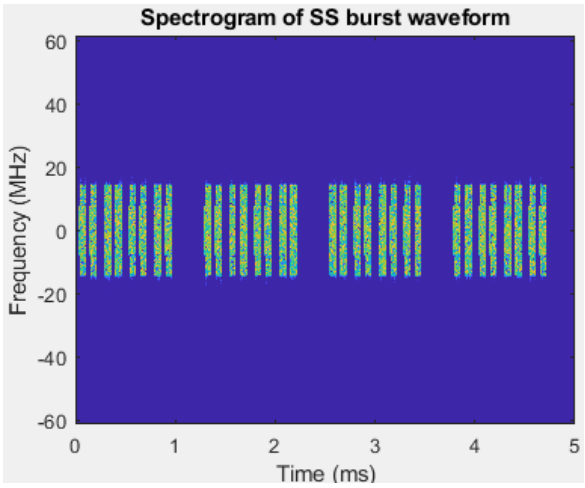

Figure 3: Spectrogram of the SSB transmission.

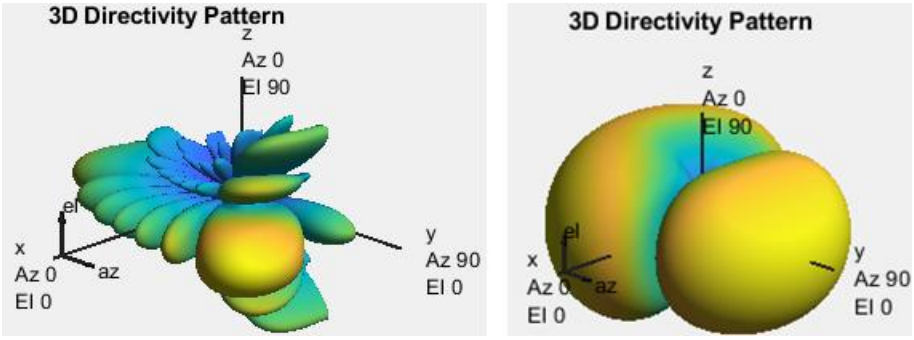

a b

Figure 4: The transmit and receive array response patterns.

For each transmit–receive beam pair, RSRP is evaluated. A beam pair with the highest RSRP is selected (e.g., Transmit #40 and Receive #9 yielding 29.0963 dBm).

The channel state information (CSI) acquisition process involves three primary types of reference signal measurements. RSRP quantifies the strength of the received CSI reference signal and serves as a key indicator of signal coverage. RSSI captures the total power received within the channel, encompassing both useful signal components and unwanted interference or background noise. RSRQ provides a normalized metric for link quality by expressing the ratio of RSRP to RSSI, offering insight into signal clarity in noisy or congested environments. Figures 5–7 demonstrate the dependence of RSRP, RSSI, and RSRQ on the interference level (Noc in dBm). Figure 8 provides an RSRP map for all beam pairs.

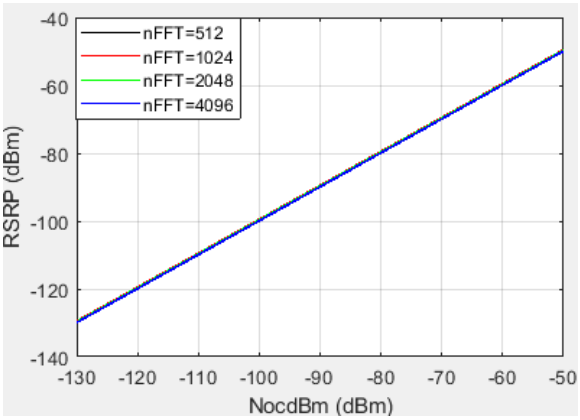

Figure 5: RSRP as a function of Noc (dBm).

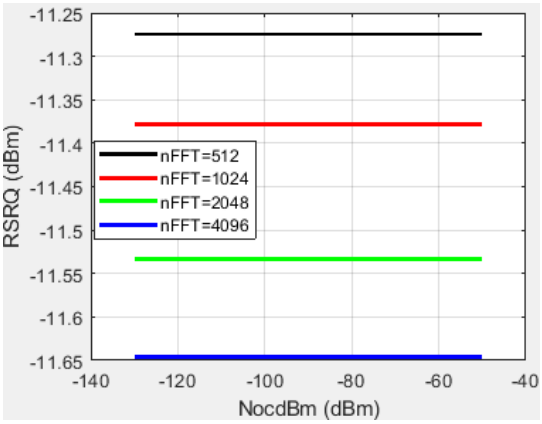

Figure 6: RSRQ as a function of Noc (dBm).

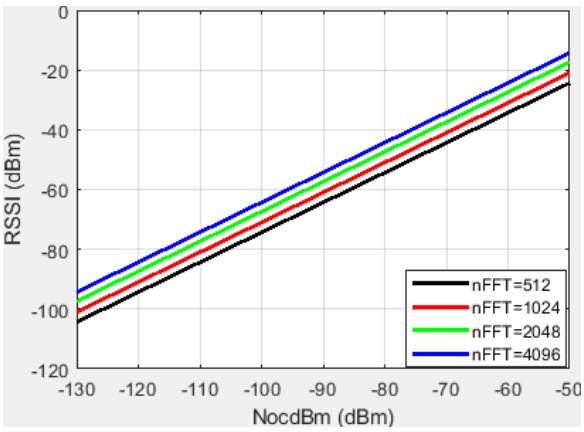

Figure 7: RSSI as a function of Noc (dBm).

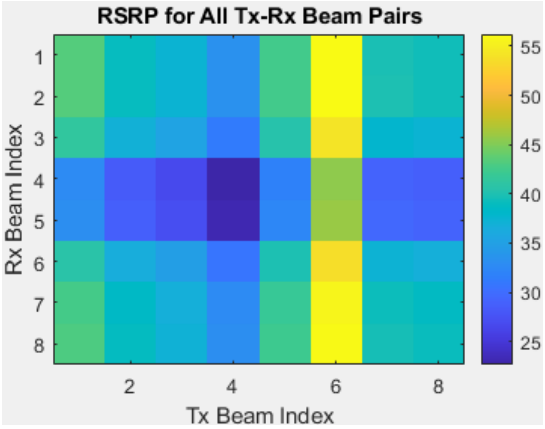

Figure 8: RSRP map of gNB–UE beam pairs.

In this study, we investigated beamforming and channel modeling using a SSB configured with a 20 ms periodicity. Each SSB occupies 240 subcarriers and spans 4 OFDM symbols [2]. The simulation environment models a MIMO channel with spatial scattering and free-space path loss. Transmitter and receiver positions are defined within a 3D Cartesian coordinate system, enabling realistic spatial geometry and directional beam interactions.

Figure 9 displays the SSB reference grid, while Figure 10 outlines beam sweeping timing for N=M=8. The dual-side sweep requires 160 ms.

To achieve beam sweeping at the transmitter, each synchronization signal (SS) [12, 15] block within the generated SSB burst is transmitted using analog beamforming. Based on the total number of SS blocks in the burst and the specified sweeping ranges, the azimuth and elevation directions for the beams are determined. Each SS block is then beamformed and transmitted in a unique spatial direction. The resulting beamformed signal propagates through a spatially selective scattering channel. At the receiver, beam sweeping is performed by sequentially receiving the transmitted beamformed SS burst across all predefined reception directions. For N transmit beams and M receive beams, the P-1 initial access procedure involves transmitting each of the N beams M times from the

gNB, ensuring that every transmit beam is captured by each of the M receive beams at the UE side. In our study, both N and M are set equal to the number of SS blocks in a single SSB burst. Figure 10 illustrates a beam-domain representation of the sweeping procedure at both the gNB and UE sides, assuming N=M=8 in the azimuth plane.

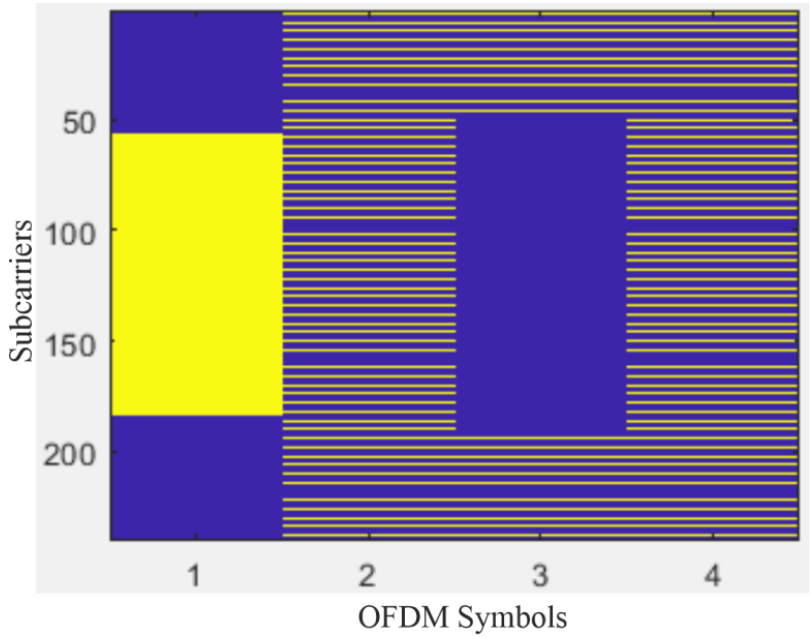

Figure 9: The transmit and receive array response patterns.

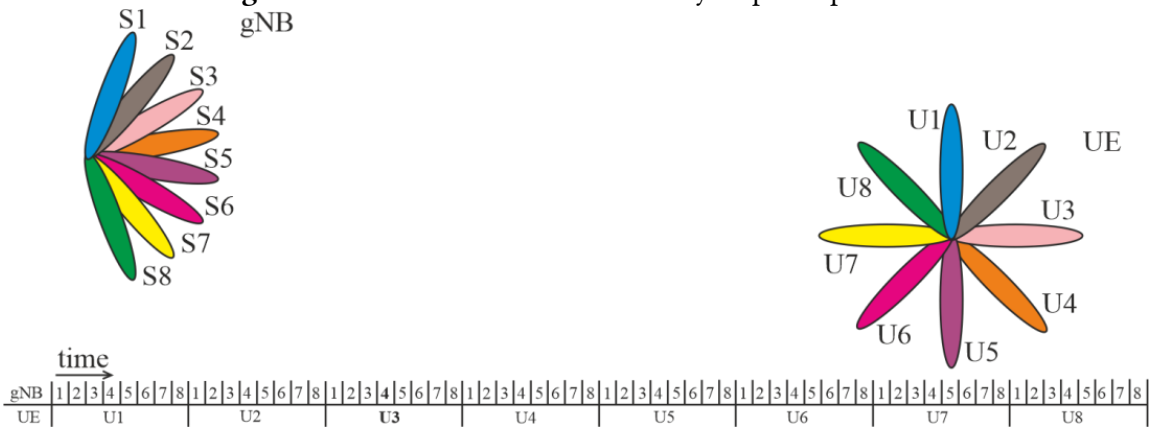

Figure 10: Beam diagram for the scans on the gNB and UE for N=M=8.

In 5G NR, a complete SSB burst—comprising 8 SS blocks—is transmitted every 20 ms. Therefore, achieving full bidirectional beam sweeping over all 8×8 beam pair combinations requires 160 ms to complete. The diagram highlights the timing structure of this dual sweeping process, where each horizontal segment corresponds to an individual SSB transmission at the gNB, and each vertical segment represents an SSB burst at the UE. This implementation realizes full bidirectional scanning across N×M time instances.

After the completion of beam sweeping and measurement on both the transmitter and receiver sides, the optimal beam pair is selected based on the highest RSRP measurement. The resulting visualizations highlight the transmit and receive beam patterns as well as the spatial scene (Figure 11). The outcomes depend on the specific beam directions used during the sweeping procedure. The spatial scene illustrates the configuration of the transmit and receive antenna arrays, the selected optimal beam pair, and the location of the scatterer.

Figure 12 presents the RSRP matrix visualization obtained in our study, allowing us to identify which transmitter-receiver pair delivers the strongest signal level.

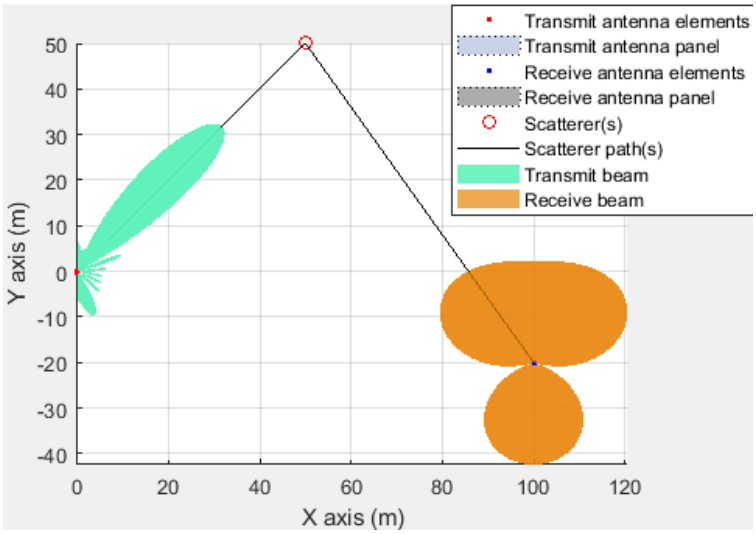

Figure 11: Directional patterns of the transmitter, receiver, and spatial scene.

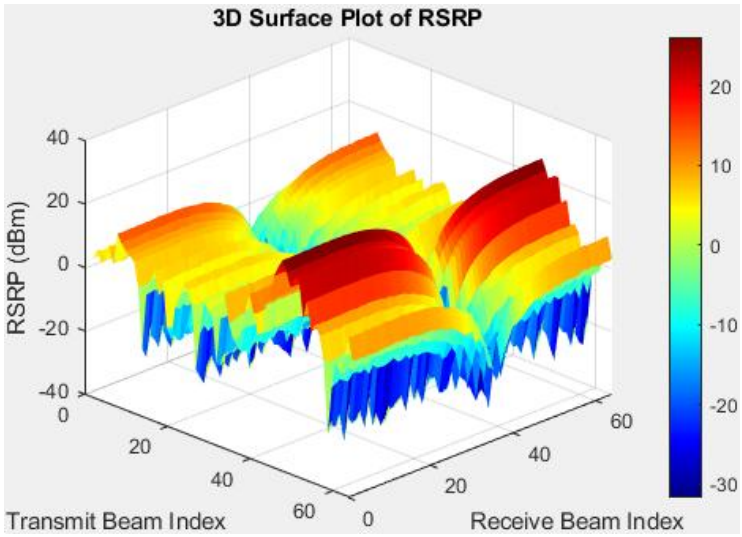

Figure 12: RSRP matrix visualization.

Next, we present the study on the downlink beam refinement procedure using the Channel State Information Reference Signal (CSI-RS). For P-2, the gNB transmits CSI-RS using narrowly focused beams. The system configuration includes a 50 MHz carrier bandwidth with 30 kHz subcarrier spacing, a 2D antenna array setup with precise location configuration, calculation of free-space path loss combined with the application of a spatial MIMO channel model (16), and receiver noise modeling (17) based on the Boltzmann constant, bandwidth, and equivalent noise temperature.

Figure 13 illustrates the key stages of the downlink beam refinement procedure processing at the transmitter.

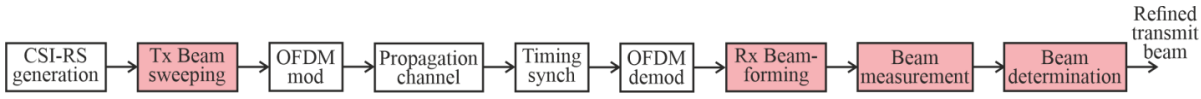

Figure 13: Key signal processing stages for procedure P-2.

Time synchronization is achieved by cross-correlating the received reference symbols with a local copy of the NZP-CSI-RS symbols. To establish the initial reception beam direction—ideally aligned, either partially or fully, with the position of the scatterer—we examine the beamwidth variation as

a function of the steering direction in a three-dimensional plane (Fig. 14). Beams pointing near the central direction of propagation exhibit narrower widths, while at the edges of the steering range (±60° in azimuth), the beam becomes wider due to stronger sidelobes. The plot in Figure 14 illustrates how the azimuthal beamwidth changes when steering across different directions.

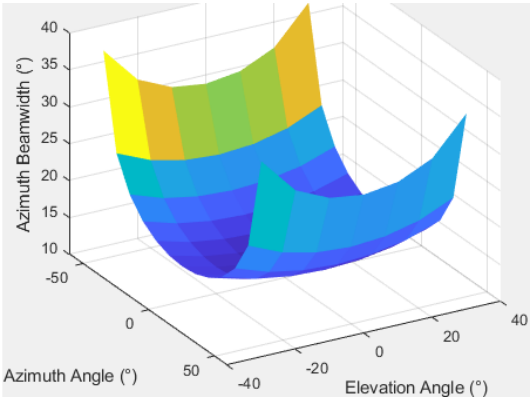

Figure 14: Beamwidth vs. steering direction.

Next, we present the constructed MIMO scattering scenario, which includes the transmit and receive antenna arrays, the positions and paths of the scatterers, as well as the radiation patterns of both the transmitting and receiving arrays (Figure 15).

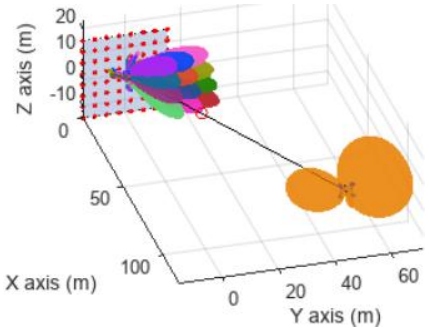

Figure 15: Transmit and receive radiation patterns with the selected optimal beam pair.

Below, we present our study on the refined beamwidth as a function of the number of transmit antennas (Figure 16).

Figure 16: Refined beamwidth vs. number of transmit antennas.

When the number of antennas in the array is a power of two, the refined beamwidths in both azimuth and elevation are equal. Once the number of antenna elements (18) exceeds 128 (2^7), further increases result in only marginal beamwidth reduction—approximately 5° when scaling from 128 to 1024 elements.

3. Neural Network for Beam Selection

In our research, a neural model [19] was developed to select beam pairs based solely on the receiver's GPS coordinates [20], following the methodology previously outlined. Assuming fixed positions for the transmitter and environmental scatterers, we built a labeled dataset: each sample paired the UE's location with the index of the actual optimal beam pair, determined via exhaustive search across all transmit–receive beam combinations.

Our neural architecture takes the receiver's spatial coordinates as input and outputs a ranked list of candidate beam pair indices. During inference, the network first proposes a set of K candidate pairs. Instead of exhaustively scanning all beams, we then evaluate only these K, calculating the average RSRP for each. The beam pair with the highest average RSRP among them is chosen as the final predicted beam.

This approach significantly reduces the search space and access latency while retaining close-to-optimal performance by leveraging location-based prediction combined with limited exhaustive evaluation.

A schematic overview of the NN training process is shown in Figure 17, whereas Figure 18 depicts the testing process.

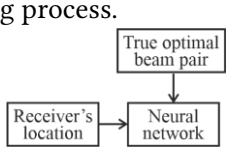

Figure 17: Schematic of NN training phase.

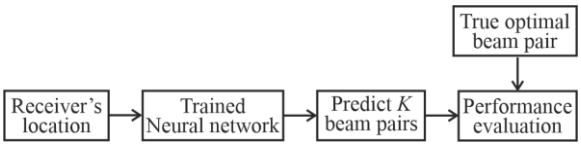

Figure 18: Schematic of NN testing phase.

We carried out the preparation for initial data generation. Receiver positions are randomly placed along the edges of a 6×6 m² area. Each receiver supports 16 transmit–receive beam pair combinations, formed using 4 analog beams at both ends and a single RF chain. The beam selection is based on an exhaustive scan across all beam pairs, conducted under AWGN conditions. The configuration remains fixed for the transmitter and scatterers in all simulations. For each receiver location, four independent channel realizations are simulated. The beam pair with the highest average RSRP is assigned as the optimal one. This label is used as the ground truth for supervised learning (Figure 19). To train a neural classifier, beam pair labels are converted into categorical values. The output space is defined for 16 classes, covering all possible combinations. Padding is applied if needed to maintain uniform dimensionality across samples. The labeled dataset reveals clear spatial grouping of beam indices, with neighboring receivers often sharing the same optimal pair. This reflects the directional properties of the environment and is shown in Figure 20.

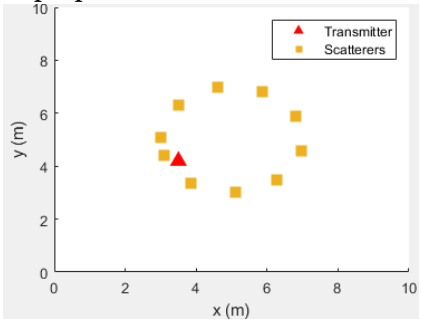

Figure 19: Schematic layout of transmitter and scatterers.

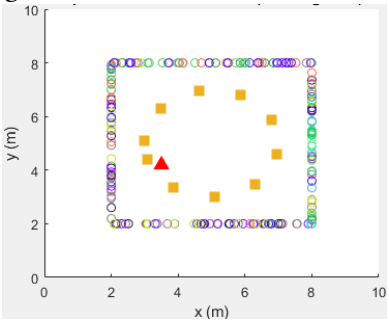

Figure 20: Visualization of optimal beam pair indices (training set).

The NN was trained using a four-layer hidden architecture, where the positions of the receivers were also incorporated as part of the input features, as illustrated in Figure 21.

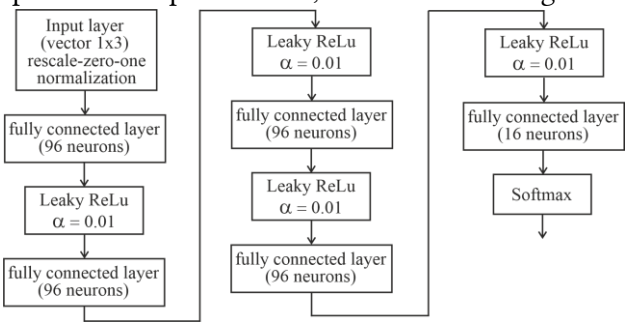

Figure 21: Architecture of a neural NN with four hidden layers.

As depicted in Figure 21, the final fully connected layer is followed by a Softmax layer [21] and subsequently by a classification layer. The activation function of the output block is the Softmax function, which is mathematically represented below:

$$y_r(x) = \frac{\exp\left((a_r(x)\right)}{\sum_{j=1}^{k} \exp\left((a_j(x)\right)} \tag{1}$$

where $0 \le y_r \le 1$ and $\sum_{j=1}^{k} y_j = 1$.

The Softmax function was used as the activation function of the output block after the final fully connected layer for multi-class classification tasks.

$$P(c_r \mid x, \theta) = \frac{P(x, \theta \mid c_r) P(c_r)}{\sum_{j=1}^{k} P(x, \theta \mid c_j) P(c_j)} = \frac{\exp\left((a_r(x, \theta)\right)}{\sum_{j=1}^{k} \exp\left((a_j(x, \theta)\right)} \tag{2}$$

where $0 \le P(c_r \mid x, \theta) \le 1$ and $\sum_{j=1}^{k} P(c_r \mid x, \theta) = 1$; $a_r = \ln(P(x, \theta \mid c_r) P(c_r)), P(x, \theta \mid c_r)$ this is the conditional probability of the sample given the class r; $P(c_r)$ is the prior probability of class.

The Softmax function, also known as the normalized exponential, can be considered a multi-class generalization of the logistic sigmoid function [22, 23]. Class weighting was applied, meaning that more frequent classes were assigned lower weights, while less frequent ones received higher weights [24]. As a result, the weights of the second hidden layer in three-dimensional space are visualized in Figure 22.

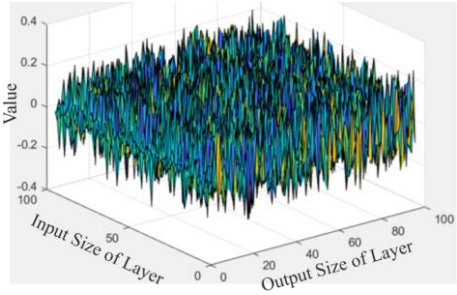

Figure 22: Second Hidden Layer Weights in 3D Space.

To evaluate Top-K accuracy [25, 26], multiple approaches were compared. Specifically, the trained NN was tested using the Top-K accuracy metric. When the receiver's location is known, the network first outputs a set of K candidate beam pairs. It then performs an exhaustive sequential search among these K pairs, selecting the one with the highest average RSRP as the final prediction. A prediction is considered successful if the truly optimal beam pair is selected as the final output. Alternatively, success also occurs if the optimal beam pair is among the K candidates proposed by the NN.

Four different beam selection strategies were evaluated, each producing K recommended beam pairs:

- Proposed NN – The primary method developed in this work, which infers K candidate beam pairs based on the input features.
- K-Nearest Neighbors (KNN) – For each test sample, this method locates the K nearest training samples based on GPS coordinates. The associated beam pairs of these training samples are then recommended. Since each training instance is linked to a single optimal beam pair, the total number of recommended beam pairs does not exceed K.
- Statistical Method – This approach ranks all beam pairs by their empirical frequency in the training dataset and selects the top K most common ones as recommendations.
- Random Selection – For each test instance, this baseline method randomly selects K beam pairs from the available pool.

Our results indicate the following: as shown in Figure 23, with K=8, the Top-K accuracy already exceeds 90%, highlighting the effectiveness of the trained NN for beam selection tasks. At K=16, each method effectively performs an exhaustive search over all 16 candidate beam pairs. The proposed NN, along with the statistical and random methods, achieves an accuracy close to 100%. In contrast, the KNN method performs approximately 20% worse, primarily because the optimal beam pair is not always present among the nearest neighbors.

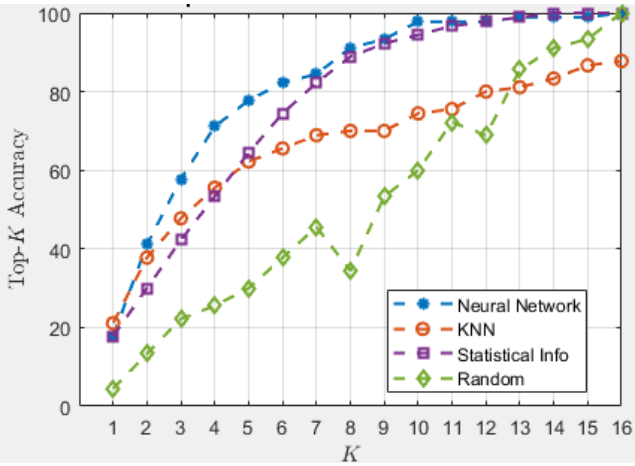

Figure 23: Results of NN testing considering the Top-K accuracy metric.

Using the test dataset, the average RSRP achieved by the NN was calculated employing four distinct methods [27, 28]. The graph (Figure 24) demonstrates that applying the trained NN [29] results in an average RSRP value approaching that of the optimal search [30].

The performance gap between KNN and optimal methods suggests that KNN may operate inefficiently, even when considering a larger set of beam pairs, such as 256. An investigation was conducted on the developed NN operating at a carrier frequency of 35 GHz, utilizing 64 synchronization signal blocks. These signal blocks are transmitted sequentially with a 5 ms interval. There are N=64 transmitting beams and M=64 receiving beams, resulting in a total of 64×64 = 4096 beam combinations. Each SSB (64 beams) is sent every 5 ms. If a mobile user scans one direction per

synchronization block, completing a full scan of all 64 receiving beams takes 64×5 ms=320 ms. Since 4096 beam pairs (transmitter–receiver combinations) must be checked, and the mobile user changes direction every 5 ms, a full two-way sweep also requires 320 ms. By employing a NN and scanning only 16 beam pairs, the maximum scanning duration reduces to 16×5 ms=80 ms, which is four times faster compared to an exhaustive search through all possible beam pairings.

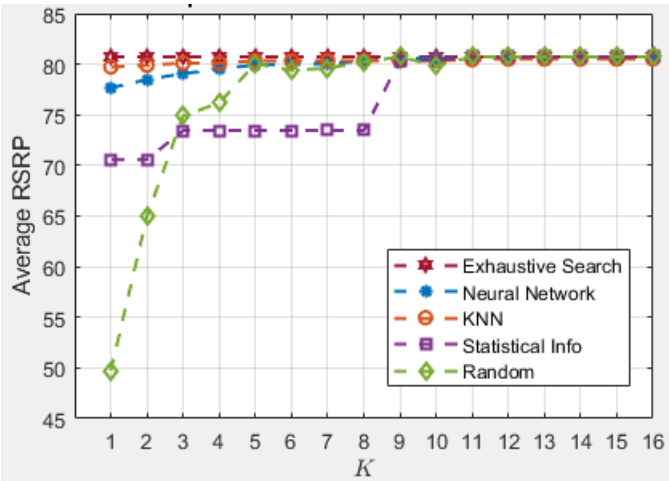

Figure 24: Dependence of average RSRP on the number of beams used for prediction in the NN.

In addition to performance optimization, the proposed NN-based beam management framework also contributes to the protection of the 5G control plane [31]. By significantly narrowing the beam search space and limiting the number of signaling exchanges required during the initial access phase, the system minimizes the exposure of synchronization and reference signals to potential interception or spoofing. This is particularly important in densely deployed networks, where frequent and repetitive control signaling can become a vector for adversarial attacks such as jamming or beam hijacking [32, 33, 34].

Moreover, leveraging spatial awareness and predictive modeling allows the network to make intelligent beamforming decisions without broadcasting full sweeping patterns. This approach inherently reduces the amount of observable overhead traffic, thereby shrinking the attack surface and improving the privacy of user equipment (UE) location and movement patterns. In this sense, the use of neural networks not only enhances efficiency but also introduces a form of implicit spatial protection — a valuable trait for modern and future wireless systems operating in adversarial environments.

Three-dimensional diagrams of mobile user and transmitter (red square) placement scenarios for training (testing) the NN are shown in Figures 25 a and b.

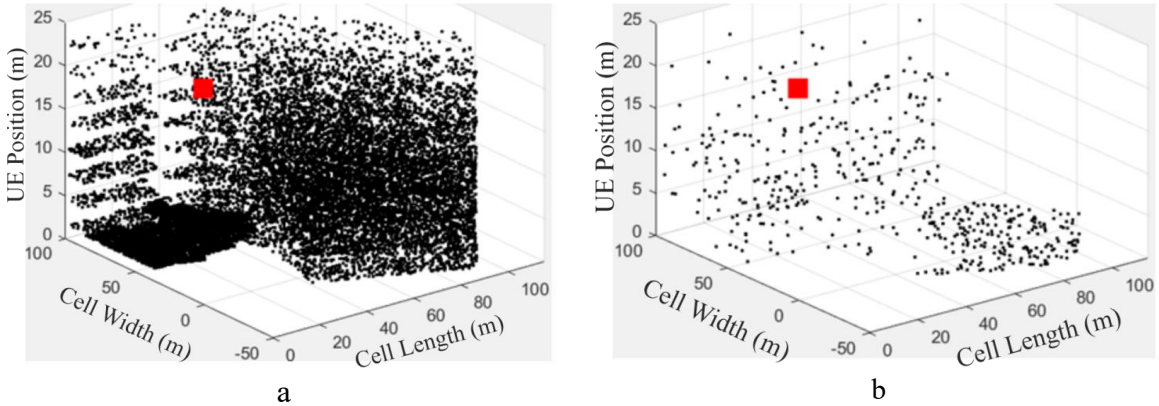

Figure 25: Three-dimensional placement scenarios of mobile users and the transmitter (red square) for the NN: (a) training setup, (b) testing setup.

A study was conducted on applying a NN to the beam selection process in 5G NR systems. The design and training of a NN capable of outputting a set of K optimal beam pairs were carried out. By limiting the exhaustive beam search to only these selected K pairs, scanning overhead can be significantly reduced.

4. Conclusion

This study investigates beam management in 5G systems with a focus on neural networks (NNs) to reduce signaling overhead and enhance secure communication. By minimizing the amount of control signaling and improving spatial transmission accuracy, the proposed approach strengthens protection against interference, eavesdropping, and other threats in the cyberspace domain. Signal processing schemes for R-1 and R-2 procedures are presented, with CSI-RS metrics (RSRP, RSSI, RSRQ) confirming minimal interference and stable propagation channels. Changing FFT points from 512 to 4096 shows negligible impact on system performance. Beam Sweeping analysis demonstrates that transmitting eight SSB blocks every 20 ms leads to a bilateral sweep time of 160 ms (8 Tx × 8 Rx) when the UE changes direction per SSB packet. Path loss analysis reveals that at 700 meters, increasing the frequency from 0.9 to 45 GHz raises path loss by 35 dB, while RMS noise at the receiver drops by 55 dB. Beamwidth studies indicate that increasing antenna elements and inter-element spacing narrows the beam. For instance, a 32-element array's beamwidth decreases by 10° when spacing increases from $\lambda/8$ to $3\lambda/2$. Beams pointed near the center of the propagation sector have narrower widths, while those at ±60° widen due to sidelobes. In elevation, beamwidth is narrowest at 0° and increases toward ±30° and ±60°, impacted by vertical array size. With 32 elements, allowable angular offset doubles from ±15° to ±30° without beam broadening; further offset increases beamwidth exponentially. For antenna arrays with power-of-two element counts, azimuth and elevation beamwidths become equal, and increasing beyond 128 elements yields only marginal (~5°) improvement. The developed NN architecture for beam selection, featuring one input, four hidden, and one output layer, was benchmarked against KNN, statistical, and random methods. The proposed NN, as well as the statistical and random strategies, achieved nearly 100% Top-K accuracy, while KNN lagged by about 20% due to suboptimal neighborhood selection. Average RSRP values show that the NN's predictions nearly match exhaustive search results, underscoring its effectiveness. For a 35 GHz setup with 64 synchronization blocks and 4096 beam pairs, exhaustive scanning requires 320 ms. Using the NN to narrow the scan to just 16 beam pairs reduces the access delay to 80 ms — a fourfold speedup.

Beyond efficiency gains, this NN-based strategy enhances the resilience of 5G communication by reducing the exposure of synchronization signals to interception or jamming. By limiting the signaling overhead during beam alignment, the system shrinks the attack surface of the control plane, contributing to a more secure and adaptive beamforming process. This work demonstrates that intelligent beam selection is not only critical for performance but also for maintaining communication integrity in modern, adversarial wireless environments — laying groundwork for scalable and protected operation in future 5G and 6G networks.

Declaration on Generative AI

The authors have not employed any Generative AI tools.

References

[1] A. Patil et al. "A comprehensive survey on spectrum sharing techniques for 5G/B5G intelligent wireless networks: Opportunities, challenges and future research directions." Computer Networks 253 (2024): 110697. https://doi.org/10.1016/j.comnet.2024.110697.

[2] I. Pyatin, J. Boiko, V. Kovtun and O. Kovtun. "Radio frequency interface quality assessment in 4G/5G: Effects of IQ imbalance, phase noise, and nonlinearities on error vector magnitude." PLoS One 20.5 (2025): e0324170. https://doi.org/10.1371/journal.pone.0324170.

[3] X. He, D. Ding and X. Y. Zhang. "An SIW-Based Wideband 5G mmWave Bandpass Filter by Using Multimode Resonator," IEEE Microwave and Wireless Technology Letters 35.4 (2025): 412-415. https://doi.org/10.1109/LMWT.2025.3533482.

[4] A. Ghosh, A. Maeder, M. Baker and D. Chandramouli. "5G Evolution: A View on 5G Cellular Technology Beyond 3GPP Release 15." IEEE Access, 7 (2019): 127639-127651. https://doi.org/10.1109/ACCESS.2019.2939938.

[5] X. Zhou, L. Chen, Y. Ruan and R. Chen. "Indoor Localization With Multi-Beam of 5G New Radio Signals," IEEE Transactions on Wireless Communications 23.9 (2024): 11260-11275. https://doi.org/10.1109/TWC.2024.3380737.

[6] E. Gures et al. "Adaptive cell selection algorithm for balancing cell loads in 5G heterogeneous networks," Alexandria Engineering Journal, 7 (2023): 621-634. https://doi.org/10.1016/j.aej.2023.04.012.

[7] N. Chukhno et al. "The Use of Machine Learning Techniques for Optimal Multicasting in 5G NR Systems," IEEE Transactions on Broadcasting, 69.1 (2023): 201-214. https://doi.org/10.1109/TBC.2022.3206595.

[8] M. S. Sim, Y. -G. Lim, S. H. Park, L. Dai and C. -B. Chae. "Deep Learning-Based mmWave Beam Selection for 5G NR/6G With Sub-6 GHz Channel Information: Algorithms and Prototype Validation." IEEE Access, 8 (2020): 51634-51646 https://doi.org/10.1109/ACCESS.2020.2980285.

[9] L. Weedage, C. Stegehuis, and S. Bayhan. "beam-align: Distributed user association for mmWave networks with multi-connectivity." Computer Networks 270 (2025): 111446. https://doi.org/10.1016/j.comnet.2025.111446.

[10] X. Yang, Y. Chen, Y. Zhao, J. Pan, J. Guo and D. Yang. "Application of KNN for Linear Array Pattern Prediction Based on the Active Element Pattern Method." IEEE Antennas and Wireless Propagation Letters, 22.5 (2023): 1134-1138. https://doi.org/10.1109/LAWP.2023.3234587.

[11] K. Venkateswararao et al. "Using UE-VBS for dynamic virtual small cells deployment and backhauling in 5G Ultra-Dense networks." Computer Networks 189 (2021): 107926. https://doi.org/10.1016/j.comnet.2021.107926.

[12] I. Pyatin, J. Boiko, O. Eromenko and I. Parkhomey. "Implementation and analysis of 5G network identification operations at low signal-to-noise ratio." TELKOMNIKA (Telecommunication Computing Electronics and Control) 21.3 (2023): 496-505. http://doi.org/10.12928/telkomnika.v21i3.22893.

[13] R. Kumar, D. Sinwar and V. Singh. "QoS aware resource allocation for coexistence mechanisms between eMBB and URLLC: Issues, challenges, and future directions in 5G." Computer Communications 213 (2024): 208-235. https://doi.org/10.1016/j.comcom.2023.10.024.

[14] J. Boiko, I. Pyatin and O. Eromenko, Analysis of Signal Synchronization Conditions in 5G Mobile Information Technologies, in: Proceedings of the 2022 IEEE 16th International Conference on Advanced Trends in Radioelectronics, Telecommunications and Computer Engineering (TCSET), IEEE Press, 2022, pp. 01-06, https://doi.org/10.1109/TCSET55632.2022.9766899.

[15] Ö. Sabuncu and B. Bilgehan. "Novel Statistical Modelling and Optimization Techniques of Fading Channel Coefficients for 5G Network Performance." Journal of Network and Systems Management 33.2 (2025): 42. https://doi.org/10.1007/s10922-025-09905-4.

[16] A. Ranjan and B. C. Sahana. Deep learning empowered channel estimation in massive MIMO: unveiling the efficiency of hybrid deep learning architecture. Journal of Ambient Intelligence and Humanized Computing 16 (2025): 375–390. https://doi.org/10.1007/s12652-025-04952-w.

[17] T. N. Guo. "Unique Measurement and Modeling of Total Phase Noise in RF Receiver." IEEE Transactions on Circuits and Systems II: Express Briefs 60.5 (2013): 262-266. https://doi.org/10.1109/TCSII.2013.2251966.

[18] I. R. Parhomey, J. M. Boiko and O. I. Eromenko. "Features of digital signal processing in the information control systems of multipositional radar." Journal of Achievements in Materials and Manufacturing Engineering 77.2 (2016): 75-84. https://doi.org/10.5604/17348412.1230101.
[19] F. M. Ghannouchi, O. Hammi and M. Helaoui, Neural Network Based Models, in: Behavioral Modeling and Predistortion of Wideband Wireless Transmitters, Wiley, New York, NY, 2015, pp.133-152, https://doi.org/10.1002/9781119004424.ch7.
[20] S.M. Hosseini and M. Jalili. "An online incremental learning support vector regression for INS/GPS integrated navigation system during long-time GPS outage." GPS Solutions 29(2025): 164. https://doi.org/10.1007/s10291-025-01900-1.
[21] A. Banerjee, E. Kumar and R. Megavath. "Learning optimal deep prototypes for video retrieval systems with hybrid SVM-softmax layer." International Journal of Data Science and Analytics (2024). https://doi.org/10.1007/s41060-024-00587-w.
[22] C. -H. Tsai, Y. -T. Chih, W. H. Wong and C. -Y. Lee. "A Hardware-Efficient Sigmoid Function With Adjustable Precision for a Neural Network System." IEEE Transactions on Circuits and Systems II: Express Briefs 62.11 (2015): 1073-1077. https://doi.org/10.1109/TCSII.2015.2456531.
[23] X. Xu, C. Liao, L. Zhou and F. Peng. "Grating Lobe Suppression of Non-Uniform Arrays Based on Position Gradient and Sigmoid Function." IEEE Access 7 (2019): 106407-106416. https://doi.org/10.1109/ACCESS.2019.2932123.
[24] O. Shynkaruk, J. Boiko and O. Eromenko, Measurements of the energy gain in the modified circuit signal processing unit, in: Proceedings of the 2016 IEEE 13th International Conference on Modern Problems of Radio Engineering, Telecommunications and Computer Science (TCSET), IEEE Press, 2016, pp. 582-584, https://doi.org/10.1109/TCSET.2016.7452121.
[25] Z. Sun, H. Huo and X. Chen. "Fast Top-K Graph Similarity Search Via Representative Matrices." IEEE Access 6 (2018): 21408-21417. https://doi.org/10.1109/ACCESS.2018.2819426.
[26] Y. Sasaki and Y. Okajima, Top-k Rule List Learning via Integer Linear Programming, in: R. Hadfi, P. Anthony, A. Sharma, T. Ito, Q. Bai (Eds.), Trends in Artificial Intelligence. PRICAI 2024. Lecture Notes in Computer Science, Springer, Singapore, 15285 (2025), pp. 16–28. https://doi.org/10.1007/978-981-96-0128-8_2.
[27] O. A. Jumaev et al. "Algorithms for increasing the efficiency of information processing in continuous channels." Journal of Physics: Conference Series 3027 (2025): 012034. https://doi.org/10.1088/1742-6596/3027/1/012034.
[28] Y. M. Boiko and R. O. Boryachok, Improving effectiveness for processing signals in data transmission channels with phase manipulation, in: Proceedings of the 2013 23rd International Crimean Conference "Microwave & Telecommunication Technology", IEEE Press, 2013, pp. 262-263. https://ieeexplore.ieee.org/document/6652818.
[29] Y. Cai, G. Chen and Z. Qiao. "Neural networks trained by weight permutation are universal approximators." Neural Networks 187 (2025): 107277. https://doi.org/10.1016/j.neunet.2025.107277.
[30] A. Ali et al. "A k-Nearest Neighbours Based Ensemble via Optimal Model Selection for Regression." IEEE Access 8 (2020): 132095-132105. https://doi.org/10.1109/ACCESS.2020.3010099.
[31] A.I. Sulyman and C. Henggeler. "Physical Layer Security for Military IoT Links Using MIMO-Beamforming at 60 GHz." Information 13.2 (2022): 100. https://doi.org/10.3390/info13020100.
[32] H. S. M. Antony and T. Lakshmanan. "Secure Beamforming in 5G-Based Cognitive Radio Network." Symmetry 11.10(2019): 1260. https://doi.org/10.3390/sym11101260.
[33] K. Tsachrelias et al. "Robust Protection of 5G MIMO Networks from Jamming Attacks via Adaptive Beamforming." Procedia Computer Science 265 (2025): 65-72. https://doi.org/10.1016/j.procs.2025.07.157.
[34] Samokhvalov, Y.Y. Developing the Analytic Hierarchy Process Under Collective Decision-Making Based on Aggregated Matrices of Pairwise Comparisons. Cybern Syst Anal 58, 758–763 (2022). https://doi.org/10.1007/s10559-022-00509-3.